FAR UV *STIS* SPECTRA OF THE WHITE DWARF REJ 1032+532 I: INTERSTELLAR LINE OF SIGHT[1]

J. B. Holberg[2]

F. C. Bruhweiler[3]

M. A. Barstow[4]

P. D. Dobbie[5]

ABSTRACT

An 1150 Å to 1725 Å echelle spectrum of the hot DA white dwarf REJ 1032+532, recently obtained with the *STIS* E140M grating, reveals numerous stellar and interstellar lines. Determinations of the interstellar column densities and abundances of C, N, O, Si and S relative to the directly measured H column are determined for this particular line of sight through the local ISM. An estimate of the electron density, $n_e = 0.11^{+0.07}_{-0.06}$, is obtained from the population ratio of the excited to ground state fine structure levels in C II. This electron volume density is compared with an independent *EUVE* measurement of the total line of sight electron column density derived from the ionization state of H and He. A path length of ∼10 pc is estimated for the region responsible for the bulk of the ISM absorption. From the observed ISM velocity components, we identify this absorbing component as the Local Interstellar Cloud (LIC) surrounding the solar system. For the LIC we find the abundances of nitrogen, oxygen and silicon relative to hydrogen to be significantly less than those characteristic of much longer lines of sight through the local ISM. The LIC abundances of these elements are very consistent with the recent determinations of Vidal-Madjar et al. (1998) for the LIC.

Subject headings: stars; individual (REJ 1032-532) – ultraviolet: stars – white dwarfs ISM ISM: abundances

1. INTRODUCTION

Hot white dwarfs are very powerful tools for the study of the Local Interstellar Medium (LISM). The brightest of these stars are relatively nearby ($\lesssim$100 pc), so that their sight lines probe only the LISM and

---

[1]Based on observations with the NASA/ESA Hubble Space Telescope obtained at the Space Telescope Science Institute, which is operated by the Association of Universities for Research in Astronomy, Inc. under NASA contract NAS 5-26555.

[2]Lunar and Planetary Laboratory, Gould-Simpson Bld., University of Arizona, Tucson, AZ 85721 holberg@argus.lpl.arizona.edu

[3]Department of Physics, Catholic University of America, Washington D.C., 20064 fredb@iacs.gsfc.nasa.gov

[4]Department of Physics and Astronomy, University of Leicester, University Road, Leicester LE1 7RH, United Kingdom mab@star.le.ac.uk

[5]Department of Physics and Astronomy, University of Leicester, University Road, Leicester LE1 7RH, United Kingdom pdd@star.le.ac.uk

on average intercept a minimum number of interstellar clouds. Just as important, however, the strong but intrinsically simple EUV and UV continua of these stars offer the best possible circumstances for the study of interstellar absorption lines, providing access to many important species over a wide range of wavelengths. In particular, the EUV band between 200 Å and 600 Å offers a unique opportunity to simultaneously determine the column densities of the two most abundant ISM elements, hydrogen and helium and to measure their ionization states. Neutral H columns are readily determined from strong Lyman continuum absorption shortward of 912 Å. Likewise, the He II column density can be determined from its Lyman edge at 228Å. The He I density can be measured for low columns by the 504 Å photoionization edge and at higher columns by autoionization features, the strongest being located at 206 Å (Rumph et al. 1994). In practice, however, all of these measurements are only possible in a single star for a restricted range of interstellar H I columns $17.9 < \log(N_H) < 19.1$. For lower column densities the He I features are often too weak to detect and for higher columns the 504 Å edge may not be visible. Barstow et al. (1997, hereafter, B97) surveyed the existing *EUVE* spectra of 18 DA white dwarfs, and were able to measure H I, He I, and He II columns for five of these, including REJ 1032+532. The primary significance of these measurements is that it was possible to directly estimate the average ionization ratios for both hydrogen and helium for these five sight lines through the LISM. These authors found that the mean H and He ionization ratios for all five stars, representing differing directions in the LISM were $\chi_H = 0.35 \pm 0.10$ and $\chi_{He} = 0.27 \pm 0.04$, where the ionization ratios are defined as χ_H = H II/(H I + H II) and χ_{He} = He II/(He I + He II). The ionization state of helium is of critical importance because of all the elements, helium should be the best indicator of non-equilibrium ionization in the LISM. It has been known for some time (Cheng & Bruhweiler, 1990; Lyu & Bruhweiler, 1996; and Vallerga, 1998) that the He ionization ratio in the LISM is too high to be explained by equilibrium photoionization alone and some non-equilibrium process must be responsible for much of the observed He ionization.

REJ 1032+532 (WD 1029+537) was discovered as a bright EUV source with the *Wide Field Camera (WFC)* during the *ROSAT* all-sky EUV survey where is was first identified as a hot DA white dwarf (Pounds et al. 1993). Available spectroscopic and photometric data (Holberg et al. 1998b, hereafter, Paper II) yield T_{eff} = 46,660 ± 500 K and log g = 7.781 ± 0.03 and place REJ 1032+532 at a consistent distance of 132 ± 7 pc. This star is among the five white dwarfs for which B97 were able to obtain direct measurements of the H I, He I, and He II interstellar column densities from the *EUVE* spectrum. From these measurements it was possible to determine the ionization state of the LISM along the line of sight to REJ 1032+532 and the other four white dwarfs. It was primarily this unique knowledge about the ionization state of the LISM that led to the inclusion of REJ 1032+532 among the white dwarfs to be observed with *Space Telescope Imaging Spectrometer (STIS)* in Cycle 7.

We present here some of the first white dwarf spectra obtained with *STIS* in echelle mode. The ISM measurements for this data set are described in §2. In §3.1 we obtain independent estimates of the neutral H column density to REJ 1032+532 from an analysis of the Lyman α profile. A re-analysis of the *EUVE* spectrum of REJ 1032+532, which incorporates the measured *STIS* photospheric abundances in the stellar spectra, is discussed in §3.2. The interstellar line-of-sight to REJ 1032+532 is described in §3.3 and the electron density and thickness of the Local Interstellar Cloud (LIC) are discussed in §3.5.

2. OBSERVATIONS

REJ 1032+532 was observed under *HST* Guest Observer Program GO7296 for two orbits on 5 February 1998. A total exposure time of 2163 s was obtained through the *STIS* $0.2'' \times 0.09''$spectroscopic slit using the E140M echelle grating. The grating was positioned at a central wavelength of 1425 Å and yielded a spectrum covering the 1150 Å to 1725 Å band at a resolution of R $\sim$ 46,000. The data (observation O4G103010) were reduced using standard *STIS* software, however, it was necessary to modify two aspects of the data reduction to achieve a satisfactory final result. First, the zero point of the wavelength scale was modified to correspond to the flight calibration data. Based on a comparison of results of the subdwarf BD +75° 325 from the *GHRS* in non-echelle modes and the *STIS* echelle data, we are confident that the SITS wavelength scale for REJ 1032+532 is accurate to within 1-2 km s^{-1}. Second, it was evident that the standard STScI reduction over-corrected the background leading to a Lyman α absorption profile with negative fluxes in its core. This was traced to a lack of an improper interorder scattered light correction used in the initial STScI software. A correction scheme was developed with the assistance of Don Lindler of the *STIS* support team at NASA/GSFC. At the time that the data reduction was performed for these spectra, very few data had been obtained using the echelle mode of the *STIS*. However, a scheme was developed using E140M data for the subdwarf BD +75° 325, which had also been extensively observed using the *GHRS* in the high resolution non-echelle modes. This allowed a means to test the technique for correcting for interorder scattered light. The preliminary correction scheme used here is accurate to within 1% of the local stellar continuum level. This scheme or a variation will be applied to future versions of STScI software.

In Table 1 we list the interstellar features found in REJ 1032+532, their apparent heliocentric velocities, equivalent widths and associated uncertainties. The laboratory wavelengths are taken from Morton (1991). The primary interstellar velocity component is characterized by C II, N I, O I, Si II, and S II features. Also present are the Si III λ1206.500 ground state transition (see Fig. 1) as is a very weak feature due to Mg II λ1239.9253. All these features have a common heliocentric velocity of +0.40 $\pm$ 0.24 km s^{-1}. There also exists a very weak secondary velocity component at $-$29.29 $\pm$ 1.65 km s^{-1}, which is evident only in three of the Si II ground state lines (see Fig. 2). The two most significant ISM lines in the REJ 1032+532 are the Si III λ1206.500 line and the C II $\lambda\lambda$1334, 1335, the later lines representing a ground state and weak excited pair (see Fig.3). These features can be used to determine the ionization state and electron density along the line of sight to REJ 1032+532 (see §3.3).

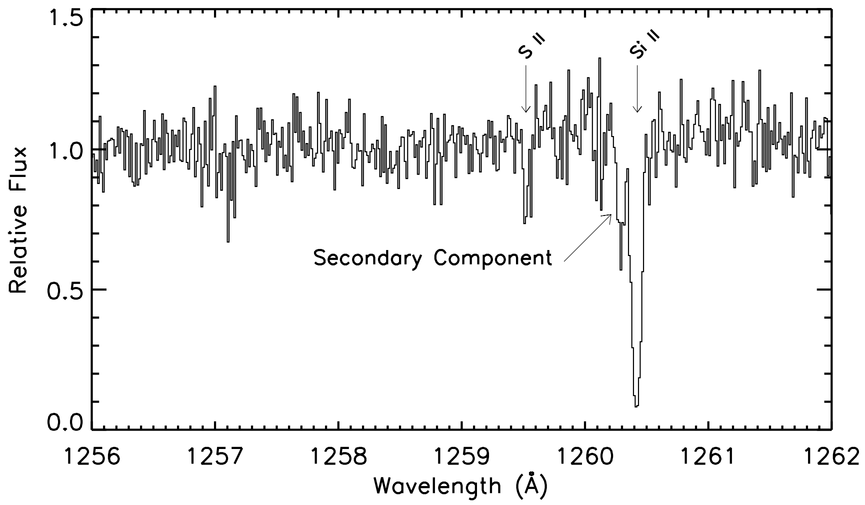

Fig. 1.— The 1255 to 1265 Å region containing the interstellar Si II λ 1260 and S II λ1259 features. Note the presence of a secondary velocity component on the blue wing of the Si II feature.

Table 1: Interstellar Lines

Ion	Lab. (Å)	Observed (Å)	V (km s^{-1})	Unc. (km s^{-1})	E.W. (mÅ)	Unc (mÅ)
			Primary Component			
N I	1199.5496	1199.5515	0.49	1.16	69	7
N I	1200.2233	1200.2220	−0.31	1.18	63	7
N I	1200.7098	1200.7095	−0.09	1.31	52	7
O I	1302.1685	1302.1786	2.33	0.64	88	4
C II	1334.5323	1334.5377	1.21	0.43	110	4
C II	1335.7076	1335.7189	2.52	3.74	12	6
Si II	1190.4158	1190.4075	−2.09	1.41	56	8
Si II	1193.2897	1193.2828	−1.72	1.13	70	7
Si II	1260.4221	1260.4169	−1.25	0.56	86	4
Si II	1304.3702	1304.3732	0.67	1.01	49	5
Si II	1526.7065	1526.7075	0.19	1.07	65	7
Si III	1206.5000	1206.4799	−5.01	3.15	28	8
S II	1259.5190	1259.5331	3.34	3.13	16	6
S II	1253.8110	1253.8206	2.28	3.53	12	6
S II	1250.5840	1250.5691	−3.57	4.07	8	5
Mg II	1239.9253	1239.9198	−1.33	2.71	7	5
		<V>	+0.40	0.24		
			Secondary Component			
Si II	1193.2897	1193.2031	−21.74	4.92	10	8
Si II	1260.4221	1260.2941	−30.46	2.27	29	6
Si II	1526.7065	1526.5543	−29.89	2.68	12	7
		<V>	−29.29	1.63		

3. DISCUSSION

3.1. Interstellar Lyman α Absorption

Our *STIS* spectrum of REJ 1032+532 permits an independent estimate of the total H I column density to REJ 1032+532 from the core of the broad stellar Lyman α profile. This is an important quantity as it permits an independent verification of an important part of the B97 *EUVE* analysis. In Fig. 4 we show the observed stellar Lyman α profile together with a model stellar atmosphere specified by the parameters T_{eff} = 46,330 ± 500 K and log g = 7.781 ± 0.03. (See Paper II). The only adjustments made to the model fluxes to match the observed stellar profile are a Doppler shift of +39.37 km s^{-1} (Paper II) and a scalar adjustment to the flux level of +0.197 mag. The latter may be explained by the light loss at the slit and the fact that the observed fluxes are based on pre-flight calibration files. The central core of the line is due primarily to H I interstellar Lyman α absorption. In Fig. 5 we show the normalized ISM absorption profile obtained by dividing the observed flux by the model flux. The small central emission component is a geocoronal H I Lyman α emission line, of equivalent width 330 mÅ and located at 1.1 km s^{-1}. Also shown

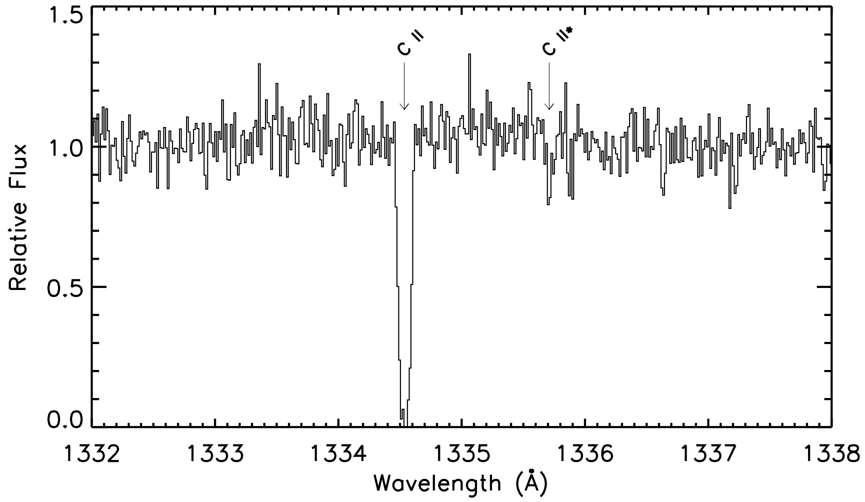

Fig. 2.— The 1332 Å to 1338 Å region containing the interstellar C II lines. The C II λ1335.7077 line is collisionally excited.

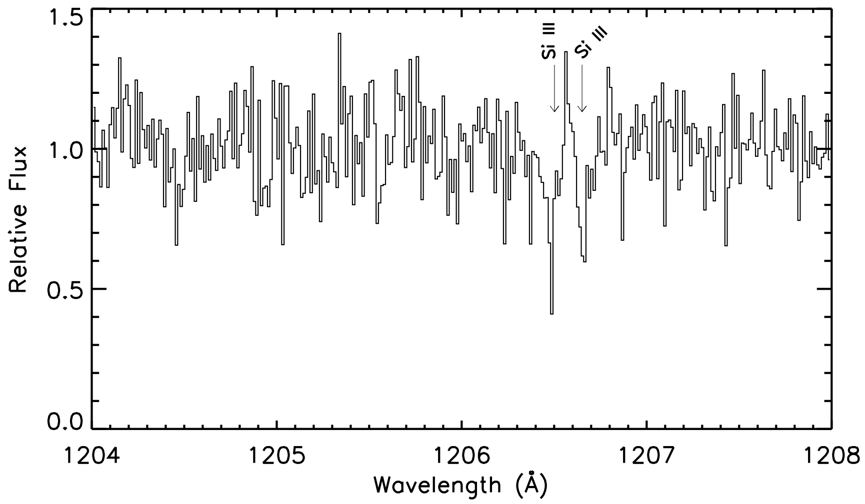

Fig. 3.— The 1204 Å to 1208 Å region containing the interstellar and stellar Si III λ1206.500 lines. The stellar line has a slanted label.

in Fig. 5, is a best fit theoretical H I Lyman α profile. The model interstellar H I absorption consists of a saturated Lorentz profile determined entirely by the total H I column, N_{HI}. The line center is fixed at the observed ISM velocity of +0.40 km s^{-1}. The fit, which was confined to a wavelength region within $\pm$ 1.6 Å of the line center and excluded the geocoronal emission component, yields a best fit value of log (N_{HI}) = 18.72 $\pm$ 0.10. Our Lyman α N_{HI} can be compared with the estimate of the continuum based on the EUV continuum measurements of B97 of log(N_{HI}) = 18.62 $\pm$ 0.05.

3.2. Reanalysis of the *EUVE* Spectrum of REJ 1032+532

The original analysis of the REJ 1032+532 *EUVE* spectrum by B97 was based on a relatively unconstrained fitting of the data to stellar and interstellar models. The stellar parameters were allowed to vary within the following optically determined limits; 44,200 K < T_{eff} < 45,300 K, 7.64 < $\log g$ < 7.77, and V = 14.46 ± 0.02. A temperature dependent mix of heavy elements, defined by the radiative equilibrium abundances of Chayer et al. (1995), were added which slightly affected the EUV opacity for REJ 1032+532. The interstellar columns for H I and He I and He II were allowed to vary freely. The corresponding best fit values for the interstellar columns and their 1σ limits are given in Table 2.

Table 2: *EUVE* Column Densities

Species	Column Density (B97)	Column Density (Re-analysis)	Comment
N_{HI}	18.62 ± 0.05	18.62 ± 0.05	Measured
N_{HII}	$18.56^{+0.09}_{-0.12}$	18.52 ± 0.08	Calculated
N_{H}	18.89 ± 0.07	18.87 ± 0.06	Calculated
N_{HeI}	$17.76^{+0.03}_{-0.04}$	$17.75^{+0.01}_{-0.02}$	Measured
N_{HeII}	$17.32^{+0.11}_{-0.14}$	$17.28^{+0.07}_{-0.10}$	Measured
N_{e}	$18.58^{+0.09}_{-0.11}$	18.54 ± 0.07	Calculated

Here we re-analyze the *EUVE* spectrum of REJ 1032+532 in a more constrained environment than that used by B97. In particular, we use a refined set of stellar parameters (see Paper II) given by T_{eff} = 46,330 ± 500 K, log g = 7.781 ± 0.03 and V = 14.455 ± 0.02. In addition, we have applied the interstellar Lyman α neutral hydrogen column density constraint discussed above. Using the same grid of stellar models discussed in B97 and the spectral fitting program XSPEC (Shafer et al. 1991) we estimate the interstellar column density for H and He. These are also given in Table 2.

3.3. *STIS* Interstellar Spectrum

The REJ 1032+532 spectrum contains two ISM velocity components, a primary component at +0.40 ± 0.24 km s^{-1} and a much weaker secondary component at −29.29 ± 1.31 km s^{-1}. Based on the observed velocities, we identify the primary component with the Local Cloud (LIC) which is the warm (∼ 7000 K) and diffuse ($n_{HI} \sim 0.1$ cm^{-3}) interstellar cloud in which the sun is embedded. Lallement et al. (1995), using ground-based and *GHRS* spectra, have precisely defined the relative velocity vector between the sun and the LIC; V = 26 ± 1 km s^{-1} in the direction (l^{II}, b^{II}) = (186°±3°, 16 °± 3°). The projection of the Lallement et al. velocity vector on the direction of REJ 1035+535 (l^{II}, b^{II}) = (157.51°, +53.24°) is +6.41 ± 1.3 km s^{-1}, approximately 6 km s^{-1} greater than the heliocentric velocity of our primary component. As mentioned previously, the wavelength scale used here should be accurate to within 1-2 km s^{-1}. The difference is therefore significant, our interpretation of this is discussed below. Because of its large velocity difference, the secondary component likely lies well beyond the LIC.

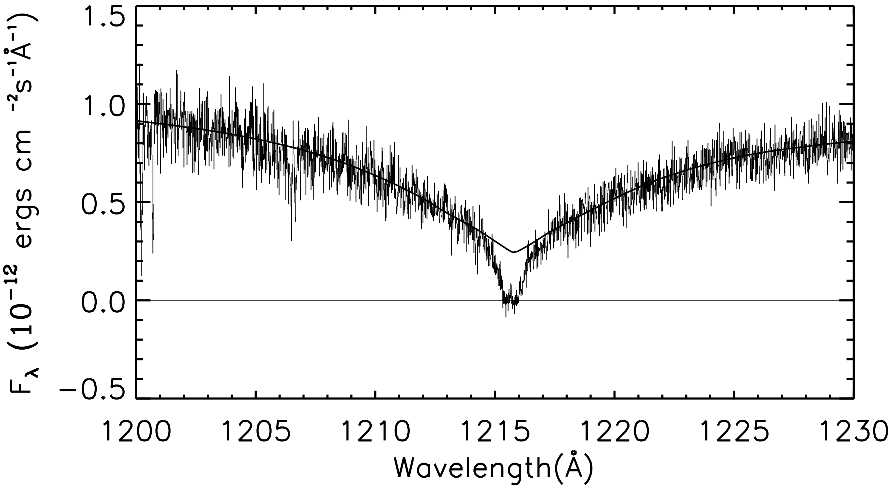

Fig. 4.— A comparison of the observed stellar Lyman α profile with a predicted model atmosphere Lyman α profile. The saturated core of the line is due to interstellar H I Lyman α absorption.

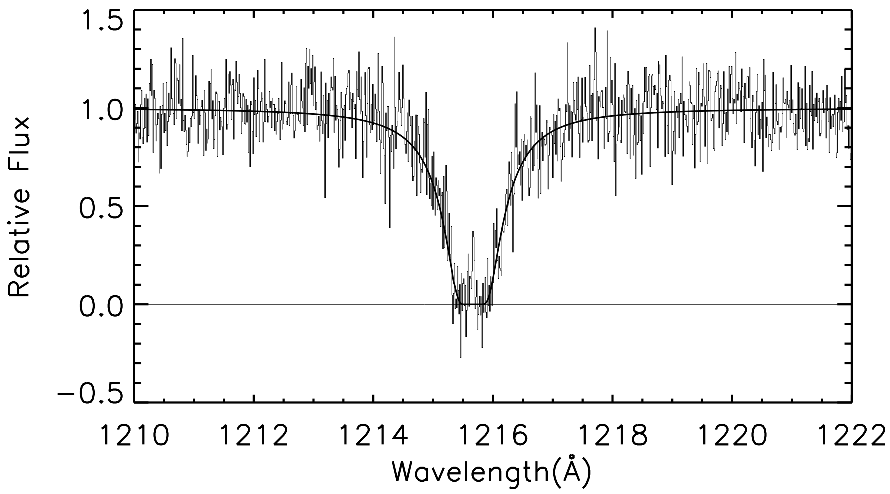

Fig. 5.— A normalized ISM Lyman α profile obtained by the ratio of observed and model stellar fluxes. The solid curve is a best fit theoretical ISM H I absorption profile for $N_{HI} = 5.2 \times 10^{18}$ cm^{-2}. The narrow emission feature near the line center is the geocoronal Lyman α line.

3.4. Interstellar Column Densities

In order to determine the column densities for the ISM species listed in Table 1 we use standard curve-of-growth (COG) techniques. In Fig. 6 we show the COG determination for the five Si II lines. The best fitting Doppler parameter is $b = 6.0 \pm 0.5$ km s^{-1}. This value is somewhat larger than the $b = 3.5$ km s^{-1} found by Wood & Linsky (1995) for Capella. We attribute our larger b value to possible unresolved velocity structure below the 6.5 km s^{-1} resolution limit of the spectrum. This would also account for the small velocity difference with respect to the LIC velocity discussed above. A similar situation can be seen in the high dispersion *GHRS* echelle grating observations (Vidal-Madjar et al. 1998) where a dominant and two subordinate ISM velocity components are resolved along the line of sight to the hot white dwarf

G191-B2B (d = 69 pc). Also perhaps relevant are the observations of a star in the general direction of REJ 1032+532, β Leo (l^{II}, b^{II},d) = (226.43°, +48.94°, 12 pc), discussed by Lallement et al. (1995). They find two and possibly three velocity components, including the LIC.

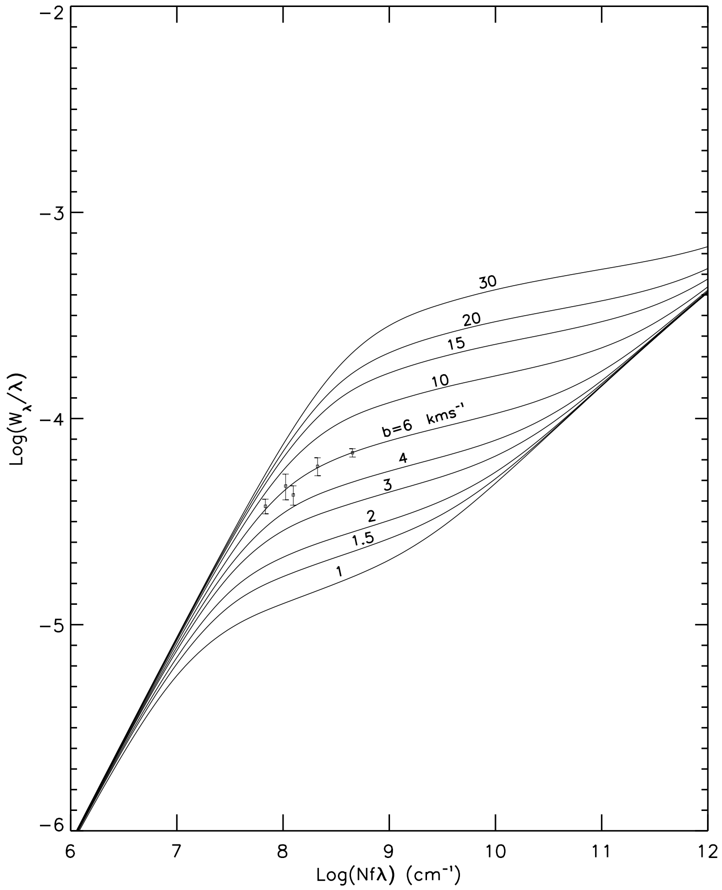

Fig. 6.— The Curve-of-Growth determination for the five observed Si II lines in the primary 'cloud'. The solid curves are labeled according to Doppler parameter. The best fitting values are log (N_{HI}) = 13.55 ± 0.07 and $b = 6.0 \pm 0.5$ km s^{-1}.

A Si II column density can be obtained for the secondary velocity component by assuming that the observed equivalent widths lie on the linear portion of the COG. The resulting silicon column, demonstrates that this 'cloud' possesses a column density approximately 7% that of the primary 'cloud'. We ignore the contribution of this secondary 'cloud' in the remaining discussion.

We adopt b = 6.0 km s^{-1} as the appropriate Doppler parameter for the remaining species in Table 1 and determine the corresponding column densities and uncertainties. In Table 3 we list the absolute and relative column densities and the depletion factors for each species. The relative column densities are computed with respect to the total hydrogen column density, $N_H = N_{HI} + N_{HII}$, while the depletion factors are with respect to the solar abundance values of Grevesse & Noels (1993). From Table 2 we find log (N_H) = 18.86 ± 0.07. We can compare our LIC abundances with recent gas phase abundances for the ISM obtained from observations of more distant O and B stars. For carbon and oxygen, Cardelli et al. (1996) find log(C/H) = −3.85 ± 0.07 and log(O/H) = −3.51 ± 0.03 compared to our values of log(C/H) = −3.89 ± 0.10 and log(O/H) = −4.09 ± 0.12. For nitrogen, Meyer et al. (1987) find log(N/H) = −4.13 ±

0.02 compared to our value of log(N/H) = -4.69 ± 0.07. In the case of silicon, Savage & Sembach (1996) find log(Si/H) = -4.98 ± 0.01 to be characteristic of the 'warm' phase of the ISM. This is approximately a factor of two larger then our value of log(Si/H) = -5.34 ± 0.05. Thus, with the exception of carbon, our LIC relative abundances are factors of 2 to 4 less than those which are characteristic of the ISM in general. In their determinations Cardelli et al., Meyer et al. and Savage & Sembach all consider much longer lines of sight and define the total hydrogen columns in terms of the neutral and molecular hydrogen components of the ISM, $N_H = 2N_{H_2} + N_{HI}$. They make no explicit allowance for the fraction of hydrogen which may be ionized, likewise our relative abundances make no allowance for the presence of molecular H_2 in the LIC. A more direct comparison is with an independent measurement of the LIC itself. Vidal-Madjar (1998) using the *GHRS* echelle A, identified three velocity components along the line of sight to the hot white dwarf G191-B2B, $(l^{II}, b^{II}) = (155.95°, +7.10°)$. One of these ('component 3') is the LIC. Vidal-Madjar obtained LIC specific relative abundances for N I, O I, Si II and Si III with respect to H I. They find, log(OI/HI) = -3.67, log(NI/HI) = -4.33, and log(Si II/HI) = -5.14, which can be directly compared with our results relative to H I, of log(OI/HI) = -3.82, log(NI/HI) = -4.42 and log(SiII/HI) = -5.07. It is apparent that, at least for these three elements, the LIC is homogeneous along the two lines of sight, which differ by $\sim$46° in galactic latitude. Curiously, the agreement for Si III is not so good: Vidal-Madjar find log(Si III/HI) < -8.14 while we detect this ion at log(Si III/HI) = -6.39.

Table 3: Interstellar Column Densities and Abundances

Ion	log N_X	$\log(N_X/H)^\dagger$	$[N_X/H]^\ddagger$
C II	15.00 ± 0.10	-3.87 ± 0.12	-0.42 ± 0.12
N I	14.2 ± 0.07	-4.67 ± 0.09	-0.64 ± 0.10
O I	14.8 ± 0.12	-4.07 ± 0.13	-0.94 ± 0.12
Si II	13.55 ± 0.07	-5.32 ± 0.09	-0.87 ± 0.10
Si III	12.23 ± 0.17	—	—
S II	13.80 ± 0.1	-5.07 ± 0.12	-0.62 ± 0.12

† Total Hydrogen: $N_H = N_{HI} + N_{HII}$
‡ Relative Depletion: [X/H] = log(X/H) - $\log(X/H)_\odot$

The existence of the interstellar Si III line is of considerable interest and requires some discussion. The presence of substantial quantities of this ion (log $(N_{SiIII}) = 12.23 \pm 0.17$) implies a high degree of ionization in the region in which it is formed, since the ionization potential of Si II is 16.346 eV. Moreover, unlike He II, Si III has a relatively high rate coefficient ($4.5\text{x}10^{-9}$ s^{-1}) for charge exchange with neutral hydrogen and is therefore unlikely to be the remnant of some past ionization event of the type suggested by Lyu & Bruhweiler (1995). Indeed, it appears, depending on the details of the ionizing radiation field, that a very high hydrogen ionization fraction ($\sim$95%) would be necessary to maintain detectable amounts of Si III. It is therefore quite doubtful that the Si III is produced in the LIC, as is the Si II. This is consistent with the previously mentioned observation of Vidal-Madjar (1998) where no Si III was detected in the LIC along their line of sight. In Table 2 it is the Si III feature which has the largest velocity difference with respect to the mean LIC velocity, indicating it is perhaps formed elsewhere.

REJ 1032+532 is not alone among white dwarfs in having a detectable Si III λ1206.500 line. At least 8 out of the 44 *IUE* DA stars analyzed by HBS show such a feature near the observed ISM velocity.

Vidal-Madjar et al. also detect the Si III line in the G191-B2B spectrum but at velocities different from that of the LIC. For example, in their 'component 2' they measure log (N_{SiIII}) = 12.34. Paradoxically, they find this component to be much cooler (~ 2000 K) then the LIC. Gry et al. (1995) had also detected several Si III and C IV velocity components in the *GHRS* spectra of ϵ CMa, along a line of sight known for very low H I column densities out to large distances (~150 pc). One of their velocity components ('component 1') which they associated with the LIC, has a Si III column of log (N_{SiIII}) = 12.30 ± 0.05, not unlike our column. Gry et al. attribute the Si III and C IV features in this component to a conductive interface between the LIC and a much hotter, highly ionized gas filling the Local Bubble. The corresponding C IV density is found to be log(N_{CIV}) = 12.5. We detect neither Si IV $\lambda\lambda$1400 nor C IV $\lambda\lambda$1550 as interstellar components in our spectra, however, our upper limits of log(N_{SiIV}) < 12 and log(N_{CIV}) < 12.5 cannot be considered inconsistent with the Gry et al. detection of C IV. In the case of Si III it appears to be difficult to generate the observed column densities with a classical conducive interface model. The sight line geometry is unknown but paths normal to the interface should produce log(N_{SiIII}) = 11.17, over a factor of ten less then observed in REJ 1032+532, G191-B2B and ϵ CMa. It is not clear that oblique paths or magnetic fields can sufficiently increase the column density.

3.5. Electron Density

The presence of the C II $\lambda\lambda$1334, 1335 (see Fig.3) lines permits an estimate of the volume density of electrons local to the line-forming region in the LISM. These lines arise respectively from the $J = \frac{1}{2}$ and $J = \frac{3}{2}$ fine structure levels of the $^2P^0$ ground state. Because the $J = \frac{1}{2}$ level lies only 0.008 eV above the $J = \frac{3}{2}$ ground state, the upper level can be collisionally populated at ISM densities and the population ratio of the two levels can be used to determined local electron density. Wood & Linsky (1997) have used these LISM C II lines superposed on the C II chromospheric emission line from Capella (d = 13.3 pc) to determine such an electron density. These same lines also occur with some frequency in the *IUE* echelle spectra of hot white dwarfs (Holberg, Barstow & Sion, 1998a), however, the λ1334 line is frequently unusable due to camera reseau marks. Below we follow closely the procedure of Wood & Linsky in estimating the electron density.

The relative populations of the two fine structure levels, (N(CII*)/N(CII)), depend on the ratio of the collisional excitation rate $n_e C_{12}$ to the radiative de-excitation rate $A_{12} = 2.29 \times 10^{-6}$ s^{-1}(Nussbaumer & Storey 1981). The resulting electron density is approximated by,

$$n_e \approx \left(\frac{N(CII^*)}{N(CII)}\right) A_{12} C_{12}^{-1}(T), \tag{1}$$

where $C_{12}(T)$ is the collisional rate coefficient. The temperature dependence of this coefficient, expressed in cgs units, is given by,

$$C_{12}(T) = \frac{8.63\times10^{-6}\Omega_{12} exp^{-\frac{E_{12}}{kT}}}{g_1\sqrt{T}}, \tag{2}$$

where $g_1 = 2$ is the statistical weight of the ground state and $E_{12} = 1.31 \times 10^{-14}$ ergs is the energy difference between the two levels. The collision strength Ω_{12} tabulated in Hayes & Nussbaumer (1984), has a value of 2.81 at 7000 K.

The column densities of the C II $\lambda\lambda$1334, 1335 lines can be determined from observed equivalent widths and their theoretical curves of growth. Assuming a Doppler velocity of 6.0 km s^{-1} for carbon, we obtain $\log N(CII^*) = 12.86^{+0.27}_{-0.31}$ and $\log N(CII) = 15.0 \pm 0.1$. From the population ratio of these two levels and the excitation and de-excitation rates discussed above, we find, $n_e = 0.11^{+0.07}_{-0.06}$ cm^{-3}. This range of densities is very similar to the $n_e = 0.11^{+0.12}_{-0.06}$ cm^{-3} range determined by Wood & Linsky (1997) for the Capella line of sight.

We can also compare our local range of n_e with the line of sight electron column density determined from the revised H and He column densities given in Table 2. This total electron column density is given by $N_e = N_{HII} + N_{HeII}$. Both here and in the determination of the H and He column densities we have explicitly assumed N_{HeIII} to be zero. Using our revised B97 values and propagating the uncertainties we obtain, log N_e = 18.52 ± 0.08. If we assume that the ISM column which we observe with *EUVE* and *STIS* is a coherent unit or 'cloud' then the ratio N_e/n_e gives an estimate of the effective path length through the 'cloud' of 10^{+12}_{-6}. The corresponding neutral hydrogen density of the LIC for this path length and the H I density of B97 is then 0.14 cm^{-3}, with in the range of values determined by others (Frisch 1996 and Wood & Linsky 1996).

Thus, the simple picture which emerges of the LISM in the direction of REJ 1032+532, is that the bulk of the observed EUV and UV absorption is due to a $\sim$ 10 pc path length through the LIC. The remaining distance to REJ 1032+532 must be much less dense and contribute very little to the observed EUV and UV absorption. With the exception of the weak secondary 'cloud', the 132 pc line of sight appears not to contain any other LIC-like clouds, although our primary cloud very likely contains unresolved velocity structure. This picture is consistent with prior observations of stars near the north galactic polar cap. Dring et al. (1997) find that the line of sight to 31 Com (l^{II}, b^{II}, d) = (114.93°, +89.58°, 90 pc) is characterized by a single velocity component and a very low H I column density, log(N_{HI}) = 17.88 ± 0.06. Likewise, HZ 43 (l^{II}, b^{II}, d) = (54.11°, +84.16°, 69 pc) and GD 153 (l^{II}, b^{II}, d) = (317.27°, +84.75°, 73 pc) have similarly low H I column densities (B97). For REJ 1032+532 then, after the sight line passes through LIC and its environs, it enters a northern galactic zone of very low density which also contains 31 Com, HZ 43 and GD 153. This zone of low density must be truly devoid of gas and not merely a region of high hydrogen ionization as proposed by Welsh, Vallerga, & McDonald (1998) for the 'β CMa Hole' where, in that direction, they find evidence for He I being the dominant ISM opacity source beyond 5 pc. A quick look at the B97 He I and He II columns for HZ 43 and GD 153 shows that these ions have column densities which imply a total He density of $n_{He} < 4 \times 10^{-4}$cm^{-3}, unless He itself is very nearly fully ionized.

In summary, we have used a recent *STIS* echelle spectrum to probe the line of sight of REJ 1032+532. We find the Lyman α determined interstellar H I column to be consistent with that found by *EUVE* from the Lyman continuum absorption. The interstellar absorption along the line of sight to REJ 1032+532 posses two distinct velocity components. The dominant column, identified with the LIC on the basis of its velocity, is responsible for approximately 93 % of the observed column density. From the ratio of the fine structure lines of C II we determine the local electron density in the LIC to be $n_e = 0.11^{+0.07}_{-0.06}$cm^{-3}. The ratio of this quantity with the total electron column density to REJ 1032+532, obtained from *EUVE*, yields a path length of 10^{+12}_{-6} pc through the LIC in this direction. The gas phase abundances of nitrogen, oxygen and silicon in the LIC is found to be significantly lower than that observed along the lines of sight to more distant O and B stars. Our LIC abundances for these elements are very similar to those found by Vidal-Madjar et al. (1998). Finally, along with several other *HST* observers, we detect a Si III line at 1206 Å which is difficult to reconcile with the LIC or a conductive interface between the LIC and the Local Bubble.

The future holds good prospects that the above analysis of the LIC and the LISM can be further refined. First, the four remaining B97 DA stars with known ISM He ionization states will be observed with *STIS* during Cycle 7. In particular, we will be able to compare these additional lines of sight to that of REJ

1032+532. If these stars reveal that the bulk of the absorption can be associated with the LIC, this would go a long way towards explaining the relatively uniform H and He ionization fractions observed by B97. It will also be possible to further investigate the chemical homogeneity of the LIC. Second, the possibility also exists of eventually extending observations of the five B97 DA stars into the FUV wavelength range between 900 Å and 1200 Å using the soon- to-be launched Far Ultraviolet Spectroscopic Explorer (FUSE). With FUSE it will eventially be possible to accurately determine the H I column densities to these five stars and to use these values to refine the *EUVE* H I and He I and He II columns. Also it will be possible to independently verify the LIC electron density using the fine structure levels corresponding to the C II $\lambda\lambda$1036, 1037 and N II $\lambda\lambda$1083, 1084 lines. Finally, FUSE will provide access to the C III λ977 and the N III λ989 resonance lines thereby providing some idea as to the extent of these ion states in the LIC.

We wish to thank Don Lindler for his assistance in deriving an interorder scattered light correction for the *STIS* E140H echelle data. We also deeply appreciate the efforts of the staff at STScI for planning the early observations of REJ 1032+532. JBH and FCB wish to acknowledge support of for this work provided by NASA through grant GO-7296 from the Space Telescope Science Institute, which is operated by the Association of Universities for Research in Astronomy, incorporated under NASA contract NAS5-26555. MAB and PDD wish to acknowledge the support of PPARC and the Royal Society thorough provision of research grants.

REFERENCES

Barstow, M. A., Dobbie, P. A., Holberg, J. B., Hubeny, I., & Lanz, T. 1997, MNRAS, 286, 58 (B97)

Cardelli, J. A., Meyer, D. M., Jura, M., & Savage, B. D. 1996, ApJ, 467, 334

Chayer, P., Vennes, S., Pradham, A. K., Thejll, P., Beauchamp, A., Fontaine, G., & Wesemael, F. 1995, ApJ, 454, 429

Cheng, K. -P., & Bruhweiler, F. 1990, ApJ, 364, 573

Dring, A. R., Linsky, J., Murthy, J., Henry, R. C., Moos, W., Vidal-Madjar, A., Audouze, J., & Landsman, W. 1997, ApJ, 488, 760

Frisch, P. C. 1996, Sp. Sci. Rev., 78, 213

Grevesse, N., & Noels, A. 1993 in Origin and Evolution of the Elements ed. N. Prantzos, E. Vangioni-Flam, M. Cassé, Cambridge Univ. Press, p 14

Gry, C., Lemmon, L., Vidal-Madjar, A., Lemoine, M., & Ferlet, R. 1995, A&A, 302.497

Hayes, M. A., & Nussbaumer, H. 1984, A&A, 134, 193

Holberg, J. B., Barstow, M. A., & Sion, E. M. 1998a ApJS (in press)

Holberg, J. B. et al. 1998b, Paper II (in preparation)

Lallement, R., Ferlet, R., Lagrange, A. M., Lemoine, R., & Vidal-Madjar, A. 1995, A&A, 308, 601

Lyu. H., & Bruhweiler, F. C. 1996, ApJ, 459, 216

Meyer, D. M., Cardelli, J.& Sofia, U. J. 1997, ApJ, 4390, L103

Morton, D. C. 1991, ApJS, 77, 119

Nussbaumer, H., & Storey, P. J. 1981, A&A, 96, 91

Pounds, K. A., et al. 1993, MNRAS, 260, 77

Rumph, T., Bowyer, S., & Vennes, S. 1994, AJ, 107, 2108

Savage, B. D., & Sembach, K. R., 1996, ARAA, 34, 279

Shafer, R. A., Haberl, F., Arnaud, K. A., & Tennant, A. F., 1991, ESA TM-09

Vallerga, J. 1998, ApJ, 497, 921

Vidal-Madjar, A., et al. 1998 (preprint)

Welsh, B. Y., Vallerga, J. V., & McDonald, K. 1998, PASP, 110, 827

Wolff, B., Koester, D., Dreizler, S., & Haas, S. 1998, A&A, 329, 1045.

Wood, B. E., & Linsky, J. L. 1997, ApJ, 474, L39

This preprint was prepared with the AAS LaTeX macros v4.0.